Article

JOURNAL OF COMPOSITE MATERIALS

Journal of Composite Materials
47(1) 51–63

DOI: 10.1177/0021998312447647
jcm.sagepub.com
SAGE

Design considerations for shape memory polymer composites with magnetic particles

Kai Yu[1], Kristofer K Westbrook[1], Philips H Kao[1], Jinsong Leng[2] and H Jerry Qi[1]

Abstract

Recent experimental investigations demonstrated that by incorporating magnetic particles into shape memory polymer matrices, a fast and remote heating of materials and shape recovery could be achieved by exposing the shape memory polymer composite to an electromagnetic field. The particles served as internal mini-antennas to transform the electromagnetic energy to inductive Joule heat, and subsequently to initiate the recovery of shape memory polymers (SMPs). In this paper, a three-dimensional computational study was carried out to study the coupling between heat transfer from spherically shaped particles and heat-induced shape recovery of SMP composites. The influence of particle size, particle volume fraction, particle heating temperature and rate to the magnetically induced shape recovery behavior was studied. The results in this paper provided a meaningful guidance for further designs and applications of the magnetic particles reinforced shape memory polymer composites.

Keywords

Shape memory behaviors, shape memory polymer composites, constitutive modeling

Introduction

Shape memory effects of shape memory polymers (SMPs) refer to the process of polymers recovering their permanent shapes in the presence of an external stimulus,[1] such as temperatures,[2–8] light[9–14] and moisture.[15,16] As an emerging class of adaptive polymers, SMPs have gained extensive research interests lately due to their excellent properties, such as high recoverable strain (up to 400%),[17] low density, low cost, easy shape programming procedure and easy control of recovery temperature, for potential applications in actuators or sensors with remarkable advantages.[18–22]

By far, various actuation methods of SMPs have been developed based on the diverse stimuli to which SMPs are responsive. Temperatures are generally considered as the most commonly used stimulus. When an SMP is exposed to a high-temperature environment, only the SMP surface is heated. Thermal energy has to be transferred to the inside of the material by thermal conduction. Heating efficiency becomes low as the dimension of SMP components becomes large. One approach to improve heating efficiency is to use internal Joule heating indirectly generated by some actuation methods. For example, it has been demonstrated recently electrically induced heating effect along the conductive pathways inside the SMPs[23–25] can improve the heating efficiency significantly. However, the intrinsic drawback of this approach is that a direct contact to the material (e.g., electrodes) is necessary, which may restrict their further applications in the environments (such as biomedical, aerospace etc.) where non-contact and distant actuation of SMPs is required.[26]

Recently, efforts have been made to improve the shape recovery rate of SMPs by using magnetic particles.[27–31] Magnetic particles in nanometer size or micrometer size have been embedded into SMPs to

[1]Department of Mechanical Engineering, University of Colorado, Boulder, CO, USA
[2]Centre for Composite Materials, Science Park of Harbin Institute of Technology (HIT), Harbin, China

Corresponding author:
H Jerry Qi, Department of Mechanical Engineering, University of Colorado, Boulder, CO, USA.
Email: qih@colorado.edu

achieve a fast and remote heating of the SMPs after being exposed to an electromagnetic field. The particles serve as internal mini-antennas to transform the electromagnetic energy to Joule heat through magnetic field-induced inductive heating of magnetic particles.[31] This approach offers some important advantages for shape recovery of SMPs. For example, heating the material could be achieved remotely. The heating rate could also be significantly increased, leading to a fast actuation. In addition, the inclusions of particles allow for medical imaging techniques, such as fluoroscopy or computed tomography scans, to detect the implanted device without additional surgeries for proper device placement and function.[27,32]

Previously, we have developed a multi-branched thermomechanical constitutive model for SMP and applied this model to quantitatively analyze the complex relaxation process of thermally responsive SMPs.[33] To capture the fundamentally different polymer relaxation modes, the constitutive model utilizes two distinct sets of nonequilibrium branches: a glassy branch representing the glassy mode of relaxation, and several rubbery branches representing the Rouse modes in the rubbery state. Different from the conventionally generalized Maxwell model, rubbery branches are not independent and therefore the required number of material parameters in the model is significantly reduced. This model was applied to study the shape recovery behavior of SMP composites with magnetic particles under a two-dimensional (2D) setting. In this paper, we expanded our previous analysis into a 3D one to understand the thermomechanical characteristics of magnetic particle-reinforced SMP composites by using the finite element simulations. We studied the influence of particle size, particle volume fraction, particle heating temperature and rate to the magnetically induced shape recovery behavior. Some considerations that should be followed in designing magnetic particles reinforced SMP composites were also discussed. The parametric studies in this paper would serve as theoretical foundations for further designs and applications of the magnetic particles-reinforced SMP composites.

Constitutive model

In this section, we present briefly the constitutive model for capturing the thermomechanical and shape memory behaviors of SMPs. More details of this model can be found in Westbrook et al.[33] It should be mentioned that this constitutive model is for the purpose of capturing the complicated thermomechanical behaviors of an SMP under various loading conditions, such as the nonequilibrium volume change, yielding behavior, post-yielding softening behavior and non-Gaussian hyperplastic equilibrium behavior of the polymer material. However, for the problem studied in this paper, not all the parameters are equally important and therefore some portions of the model can be neglected. Discussions on the importance of individual modeling components to the shape memory behavior are beyond the scope of this paper and will be reported in the future.

Overall model description

Figure 1 shows a one-dimensional rheological representation of the model. A thermal expansion component is arranged in series with mechanical elements, which consist of an equilibrium branch and several nonequilibrium branches placed in parallel. The equilibrium branch is a hyperelastic spring to represent the equilibrium behavior of SMPs. Each nonequilibrium branch is a nonlinear Maxwell element with an elastic spring and a dashpot placed in series. In the nonequilibrium branches, one is used to represent the relaxation behavior of the glassy mode, which describes the structural or segmental relaxation of polymers. The remaining branches are used to represent the relaxation processes in the rubbery state. τ_g represents the relaxation time of the glassy branch and τ_i represents the relaxation time in the i-th rubbery branch.

As demonstrated by Holzapfel,[34] the total deformation gradient of the model $\mathbf{F}$ can be decomposed as:

$$\mathbf{F} = \mathbf{F}_M \mathbf{F}_T, \tag{1}$$

where $\mathbf{F}_M$ is the mechanical deformation gradient and gives rise to stresses. $\mathbf{F}_T$ is the thermal deformation gradient. The total Cauchy stress $\boldsymbol{\sigma}$ is

$$\boldsymbol{\sigma} = \boldsymbol{\sigma}_{eq} + \boldsymbol{\sigma}_g + \sum_{i=1}^{m} \boldsymbol{\sigma}_r^i, \tag{2}$$

where $\boldsymbol{\sigma}_{eq}$, $\boldsymbol{\sigma}_g$ and $\boldsymbol{\sigma}_r^i$ are the Cauchy stresses in the equilibrium branch, the glassy branch and in the i-th rubbery branch, respectively.

Thermal expansion

The thermal expansion is assumed to be isotropic, i.e.

$$\mathbf{F}_T = J_T \mathbf{I}, \tag{3}$$

where $\mathbf{I}$ is the second-order identity tensor. J_T is the volume change due to thermal expansion/contraction and is defined as

$$J_T = \frac{V(T,t)}{V_0}, \tag{4}$$

where $V(T,t)$ is the volume at time t and temperature T. V_0 is the reference volume at the reference

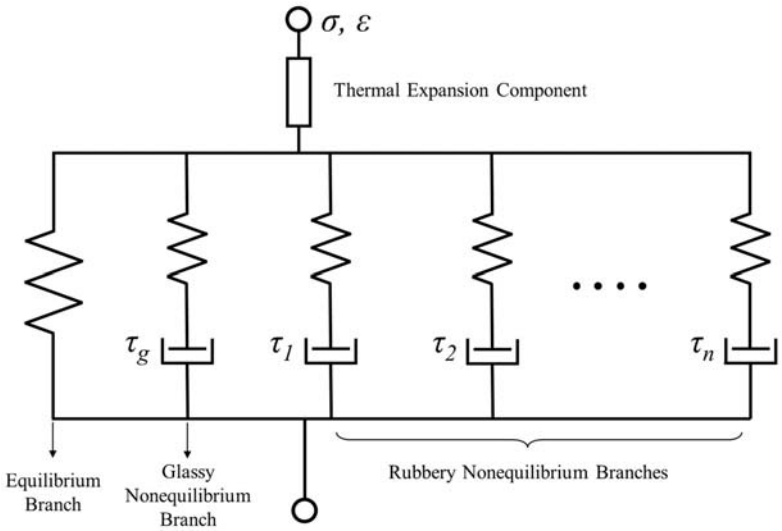

Figure 1. 1D rheological representation of the proposed model.

temperature T_0. For amorphous polymers, the volume change J_T is

$$J_T = [1 + 3\alpha_r(T - T_0)](1 + \delta), \tag{5}$$

where α_r is the linear coefficient of thermal expansion (CTE) in the rubbery state and δ characterizes the deviation of volume from equilibrium volume[35–37] and

$$\delta = \frac{V(T,t)}{V_{eq}(T)} - 1, \tag{6}$$

where $V_{eq}(T)$ is equilibrium volume and is calculated as

$$V_{eq}(T) = [1 + 3\alpha_r(T - T_0)]V_0, \tag{7}$$

δ is calculated by the well-known KAHR 33-parameter[38] (described in Appendix A).

Equilibrium branch

The Cauchy stress tensor in the equilibrium branch uses Arruda-Boyce eight chain model,[39] i.e.

$$\boldsymbol{\sigma}_{eq} = \frac{nk_BT}{3J_M}\frac{\sqrt{N}}{\lambda_{chain}} L^{-1}\left(\frac{\lambda_{chain}}{\sqrt{N}}\right)\overline{\mathbf{B}}' + K(J_M - 1)\mathbf{I}, \tag{8}$$

where n is the cross-linking density, k_B is Boltzmann's constant, T is the temperature and N is the number of Kuhn segments between two cross-link sites (and/or strong physical entanglements). The temperature-dependent shear modulus $\mu_r(T)$ of the elastomer (which is an indication of entropic elasticity) is given by nk_BT, where n is the cross-linking density and k_B is the Boltzmann constant. K is the bulk modulus and is typically two to three orders of magnitudes larger than μ_r to ensure material incompressibility. The deviatoric part of the isochoric left Cauchy-Green tensor is given by $\overline{\mathbf{B}}' = \overline{\mathbf{B}} - 1/3\mathrm{tr}(\overline{\mathbf{B}})\mathbf{I}$ where $\overline{\mathbf{B}} = \overline{\mathbf{F}_M}\overline{\mathbf{F}_M}^{\mathrm{T}}$ and $\overline{\mathbf{F}_M} = J_M^{-1/3}\mathbf{F}_M$. The stretch of each chain in the eight-chain network is given by $\lambda_{chain} = \sqrt{tr(\bar{\mathbf{B}})/3}$ and L is the Langevin function defined as $L(\beta) = \coth\beta - 1/\beta$.

Nonequilibrium branches

It is assumed that the viscoelastic behaviors in all nonequilibrium branches follow the same flow rules but with different relaxation times. For the *i-th* branch ($i = 1, \ldots, m+1$ and $i = m+1$ represents the glassy branch), the mechanical deformation gradient can be further decomposed into an elastic part and a viscous part

$$\mathbf{F}_M^i = \mathbf{F}_e^i\mathbf{F}_v^i. \tag{9}$$

The Cauchy stress can be calculated using $\mathbf{F}_e^i$,

$$\boldsymbol{\sigma}^i = \frac{1}{J_e^i}\left[\mathbf{L}_e^i(T) : \mathbf{E}_e^i\right], \tag{10a}$$

with

$$J_e^i = \det\left(\mathbf{F}_e^i\right),\ \mathbf{E}_e^i = \ln\mathbf{V}_e^i,\ \mathbf{V}_e^i = \mathbf{F}_e^i\mathbf{R}_e^iT, \tag{10b}$$

and $\mathbf{L}_e^i(T)$ is the fourth order isotropic elasticity tensor, which is taken to be temperature-independent in general, i.e.

$$\mathbf{L}_e^i(T) = 2G^i\left(\mathbb{I} - \frac{1}{3}\mathbf{I}\otimes\mathbf{I}\right) + K^i\mathbf{I}\otimes\mathbf{I}, \tag{11}$$

where $\mathbb{I}$ is the fourth order identity tensor, G^i and K^i are shear and bulk moduli of the i-th branch, respectively.

For the rubbery nonequilibrium branches, it is assumed that all the rubbery branches have the same shear modulus, i.e.

$$G^i(T) = n_R k_B T \quad \text{for } 1 \le i \le m, \tag{12}$$

where n_R is the cross-linking density for the nonequilibrium rubbery branches associated with the Rouse modes.[40] Since the bulk modulus is used to enforce a nearly incompressible condition, $K^i(T)$ is chosen to be equal to K in the equilibrium branch (equation (8)).

For the glassy nonequilibrium branch ($i = m+1$), the shear modulus is taken to be independent of temperature, i.e.

$$G^{m+1}(T) = \mu_g, \tag{13a}$$

and $K^{m+1}(T)$ is calculated through $G^{m+1}(T)$ using the Poisson ratio $v^{m+1} = v_g$,

$$K^{m+1}(T) = \frac{2(1+v_g)}{3(1-2v_g)}\mu_g, \tag{13b}$$

To obtain $\mathbf{F}_v^i$ in equation (9), the flow rule in the Maxwell element should be defined. Typically for inelastic materials,[34] the Mandel stress is used to drive the viscous flow. In each nonequilibrium branch ($1 \le i \le m+1$), the Mandel stress is given by

$$\mathbf{M}^i = J_e^i \mathbf{C}_e^i \left(\mathbf{F}_e^i\right)^{-1} \boldsymbol{\sigma}^i \left(\mathbf{F}_e^i\right)^{-T} \tag{14}$$

where $\mathbf{C}_e^i = \mathbf{F}_e^{iT}\mathbf{F}_e^i$ is the right Cauchy-Green deformation tensor. The viscous flow $\dot{\gamma}_v^i$ is given by

$$\dot{\gamma}_v^i = \frac{\overline{M^i}}{G^i(T)\tau_M^i\left(T, \overline{M^i}\right)}, \tag{15}$$

where the equivalent shear stress is defined as

$$\overline{M^i} = \left[\frac{1}{2}\left(\mathbf{M}^i\right)' : \left(\mathbf{M}^i\right)'\right]^{1/2}, \tag{16}$$

where $\left(\mathbf{M}^i\right)' = \mathbf{M}^i - 1/3\mathrm{tr}\left(\mathbf{M}^i\right)\mathbf{I}$. In equation (15), the temperature and stress-dependent material stress relaxation time $\tau_M^i\left(T, \overline{M^i}\right)$ will be discussed in the next section. The viscous stretch rate $\mathbf{D}_v^i$ is constitutively prescribed to be

$$\mathbf{D}_v^i = \frac{\dot{\gamma}_v^i}{\sqrt{2}\,\overline{M^i}}\mathbf{M}^i. \tag{17}$$

As discussed previously in Boyce et al,[41] $\mathbf{D}_v^i$ can be made equal to the viscous spatial velocity gradient $\boldsymbol{l}_v^i = \dot{\mathbf{F}}_v^i\left(\mathbf{F}_v^i\right)^{-1}$ by ignoring the spin rate $\mathbf{W}_v^i$ and therefore

$$\dot{\mathbf{F}}_v^i = \mathbf{D}_v^i \mathbf{F}_v^i. \tag{18}$$

Relaxation time and time–temperature shift factor

According to the thermorheological simplicity principle,[40]

$$\tau_M^i(T) = \tau_0^i a_T(T) \quad \text{for } i = 1, \ldots, m+1, \tag{19}$$

where $a_T(T)$ is the time-temperature superposition shift factor and τ_0^i is the relaxation time at the reference temperature when $a_T(T) = 1$. At temperatures around or above T_g, the WLF equation[42] is applied,

$$\log a_T = -\frac{C_1(T - T_M)}{C_2 + (T - T_M)}, \tag{20a}$$

where C_1 and C_2 are material constants and T_M is the WLF reference temperature. When the temperature is below T_g, $\alpha_T(T)$ follows the Arrhenius-Type behavior[43]:

$$\ln \alpha_T(T) = -\frac{AF_c}{k_b}\left(\frac{1}{T} - \frac{1}{T_g}\right), \tag{20b}$$

where A and F_c are material constants, k_b is Boltzman's constant.

For the glassy branch ($i = m+1$), the imposed stress also changes the relaxation time because of stress-induced yield-type behavior. The relaxation time can be evaluated by an Eyring type of function,[44] i.e.

$$\tau_M^{m+1}\left(T, \overline{M^{m+1}}\right) = \tau_0^{m+1} a_T(T) \exp\left(-\frac{\Delta G}{k_B T}\frac{\overline{M^{m+1}}}{s}\right), \tag{21}$$

where $\tau_0^{m+1} = \tau_0^g$ is the material relaxation time at the temperature when $a_T(T) = 1$, ΔG is the activation energy and s is the athermal shear strength representing the resistance to the viscoplastic shear deformation in the material.

For the rubbery branches ($i = 1, \ldots, m$), the relaxation behavior could be modeled by the Rouse model where the macromolecular chain is divided into several entropic segments. The relaxation times associated with these Rouse modes are given by,[40]

$$\tau_0^i = \frac{\tau_R}{i^2} \quad \text{for } i = 1, \ldots, m. \tag{22}$$

Finite element modeling

The above-described constitutive model was implemented as a user material subroutine (UMAT) in the finite element software package ABAQUS (Simulia, Providence, RI). To model the magnetic particle reinforced SMP, we assumed that the magnetic particles of spherical shape are uniformly distributed within the SMP matrix (Since we assume that the magnetic particles of spherical shape are uniformly distributed in the matrix, the representative volume element (RVE) predicts the average behaviors of the real composites. Any structure parameters in the real material that deviate from their average values will cause RVE deviate from real material behaviors. If a large deviation exists, one would consider a large size RVE where more structure information can be included. For example, if the particle sizes show a large standard deviation, one may consider an RVE with a few particles of different sizes. This, of course, will inevitably increase the computational expense.). An RVE was then constructed in a 3D setting as shown in Figure 2(a), where d is the diameter of the filler and $2a$ is the RVE edge length as shown. For the convenience for the following discussions, point A is marked on the 3D RVE at one of the farthest points from the magnetic particle heating surface.

The magnetic particles volume fraction ϕ_{3D} can be derived according to the RVE geometry as

$$\phi_{3D} = \frac{\pi d^3}{48a^3}. \tag{23}$$

In the following parametric studies, the magnetic particle diameter was varied over a few decades, and the corresponding RVE size under a specified particle volume fraction was calculated according to equation (23).

Due to the symmetry of the 3D RVE, it was therefore feasible to analyze only one eighth of the RVE with proper thermal and mechanical boundary conditions applied on the sectional surfaces. A representative finite element mesh for the 3D RVE is shown in Figure 2(b) for a 1% volume fraction and a filler diameter of 400 μm.

The finite deformation analysis of the 3D RVE was coupled with heat transfer by using the coupled heat-displacement analysis in ABAQUS. For the SMP matrix, the C3D8HT elements were used for analysis, which is featuring with eight-node thermally coupled brick, trilinear displacement and temperature analysis, and hybrid with constant pressure element. Following Westbrook et al.,[45] for the acrylate-based SMP, it has a heat capacity, density and conductivity of 640 J/(kg°C), 1050 kg/m^3 and 0.15 W/(m°C), respectively. For the rest material parameters defined in the constitutive relations,

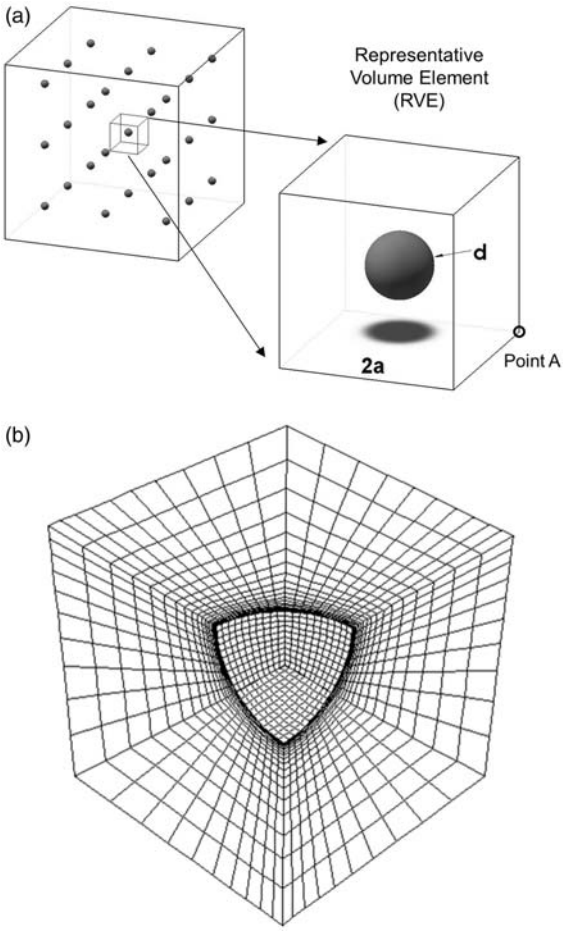

Figure 2. (a) The 3D representative volume element (RVE) for a magnetic particles reinforced shape memory polymer (SMP) composite. Point A represents one of the farthest points from the magnetic particle heating surface on the 3D RVE. (b) Finite element model mesh for the 3D RVE for a filler volume fraction of 1% and a filler diameter of 400 μm.

they were fitted with experiments on the acrylate-based SMP, as detailed in Westbrook et al.[33] The fitted material parameters of SMP are described and listed in Table 1. It should be noted that although the specific values presented in the results depend on the model material parameters in Table 1, the general trend observed in *Results* Section should be applicable to most amorphous SMPs.

Since the magnetic particle is usually a ceramic material, which has a much higher modulus than the SMP, it was considered as a rigid partial spherical surface in the model. The particle heating effect was then represented by the temperature boundary condition on this rigid surface. The thermomechanical history of the SMP composite was similar as previously used[46,47] and is shown in Figure 3. The 3D RVE was initially preheated to the programming temperature T_d, and compressed by a rigid plate to a target strain at a specified loading rate. The contact property between the 3D

Table 1. Model parameters

Description	Parameter	Value
Thermal component parameters		
Glass transition temperature	T_g (°C)	40
Linear rubbery coefficient of thermal expansion	α_r (1/°C)	2.35×10^{-4}
Linear glassy coefficient of thermal expansion	α_g (1/°C)	1.15×10^{-4}
Structural glass transition temperature	T_v (°C)	40
Material temperature parameter	θ (1/°C)	0.7
Material partition parameter	x (–)	0.7
Structural relaxation time	τ_v (s)	1×10^{-3}
Equilibrium branch parameters		
Cross-linking density	n (m^{-3})	1.7×10^{26}
Number of Kuhn segments between two crosslinks	N (–)	2.49
Bulk modulus	K (Pa)	1×10^9
Nonequilibrium rubbery branch parameters		
Cross-linking density	n_R (m^{-3})	1×10^{26}
Rouse mode longest relaxation time	τ_R (s)	1×10^5
Nonequilibrium glassy branch parameters		
Shear modulus	μ_g (Pa)	370×10^6
Poisson ratio	v_g (–)	0.4
Initial material relaxation time	τ_o^g (s)	60
Zero stress level activation energy	ΔG (J)	5×10^{-20}
Initial shear strength	s_0 (Pa)	55×10^6
Saturation shear strength	s_s (Pa)	24×10^6
Prefactor parameter	h_0 (Pa)	400×10^6
Time–temperature shifting parameters		
WLF reference temperature	T_M (°C)	30
WLF constant	C_1 (–)	17.44
WLF constant	C_2 (°C)	51.6
Pre-exponential Arrhenius factor	$AF_c k_B^{-1}$ (K)	−15500

RVE and the plate was simplified as frictionless and hard contact. It was then held to relax before the temperature was lowered to the shape fixing temperature T_L at a specified cooling rate. Once the fixing temperature was reached, the RVE was held to stabilize at the low temperature. The rigid plate was then removed. In the free recovery process, the shape (or strain) recovery was induced under the action of magnetic particle heating effect. Since the focus of this paper is the recovery behavior of SMP, we neglected the details on how magnetic energy was converted to thermal energy and assumed that magnetic particle can be heated with a prescribed temperature-time profile. For the thermal boundary conditions, all the surfaces were applied with an adiabatic boundary condition except the spherical surface representing the rigid magnetic particle. During the pre-heating and cooling processes of the 3D RVE, all the nodal temperatures in the model were prescribed. During heating, only the partial spherical surface was heated to mimic the rise of temperature of magnetic particles due to magnetic field. In the following parametric investigations, the programming temperature (T_d) and shape fixing temperature were fixed at 40°C and 20°C, respectively, for all the cases, while the particle heating temperature (T_H) and the particle heating rate were varied, respectively.

Results

It is reasonable to assume that the total time for the shape recovery of an SMP magnetic particle composite should be determined by the times for the temperature rise in the particles to the targeted temperature, for heat transfer from the particles to the SMP and for the SMP matrix to recovery. In this paper, the focus is on the heat transfer and matrix material recovery. Therefore, unless otherwise mentioned, we assumed that the particles can be heated to the targeted temperatures instantaneously (It should be noted that the results presented will change if this assumption is relaxed. This can be seen in section *Influence of particle heating temperature and rate on the shape recovery rate* when the particle temperature is ramped at a certain thermal rate. Therefore, the assumption of instantaneous heating represents an extreme case.). In the finite element model, this was achieved by ramping the temperatures of the nodes on the spherical surface representing magnetic particle to the target recovery temperature (50°C) in 0.1 ms in the recovery step.

Time-dependent recovery ratio of the SMP composite

In this section, the time-dependent shape recovery behaviors of the magnetic particle reinforced SMP composite from the finite element simulation are presented. As a representative case, the particle volume fraction is selected as 1% and the particle diameter is 400 μm. During the programming process, the total compressive strain, the loading rate and the cooling rate were set as 0.2, 0.01/s and 1.67°C/min, respectively. As proposed by Lendlein and Langer,[48] the amount of deformation recovered during a free recovery test can be quantified by using a normalized strain measurement. A strain recovery ratio $R_r = 1 - \varepsilon(t)/\varepsilon_{\max}$ is used where $\varepsilon_{\max} = 0.2$ is the compressive strain at the

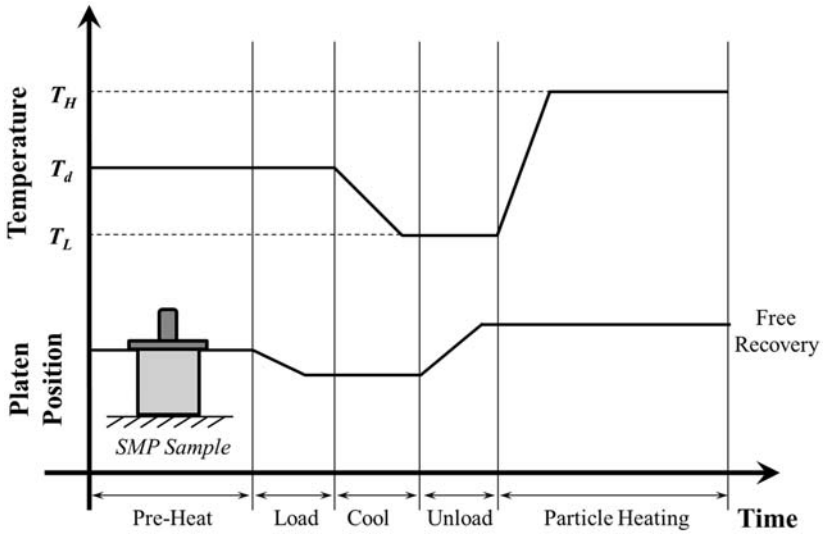

Figure 3. The thermomechanical history of the 3D representative volume element (RVE) followed in the finite element analysis.

start of the heating step and $\varepsilon(t)$ is the time-dependent strain. The time for a full shape recovery was taken to be when the strain recovery ratio reached 95%.

Figure 4 shows the strain recovery ratio and temperature evolution of the 3D RVE during the free recovery process, where the temperature is collected on point A. It is observed that within the small initial time period (~7 s) of the particle heating, no noticeable strain recovery is observed. During this time period, heat transfer within the material dominates, and significant shape recovery behavior is not triggered only after the average temperature of SMP matrix is ramped above a critical value. Detailed study on the onset temperature of shape recovery will be presented in the following section. When the thermal transmission within the 3D RVE ends, the shape recovery in the SMP material starts. At $t = 14.7$ s, the strain recovery ratio reaches 95%. After 20 s, the permanent shape of the 3D RVE is totally recovered.

The temperature distributions within the 3D RVE are plotted as contours in Figure 5. Within the first 7.2 s since the beginning of particle heating, thermal energy is transferred from the particle surface to the outer boundaries of RVE. The temperature decreases along the thermal conductive pathways. Since the modulus of SMP is very sensitive to temperatures in the vicinity of T_g, the material near the outer surface has a much higher modulus than the material inside and therefore confines the material inside. This confinement has two effects. First, shape recovery does not occur until the temperature on the outer surface of the RVE is high so that the material on the outer surface starts to recover. Therefore, the shape recovery rate is dominated by the recovery of the material at

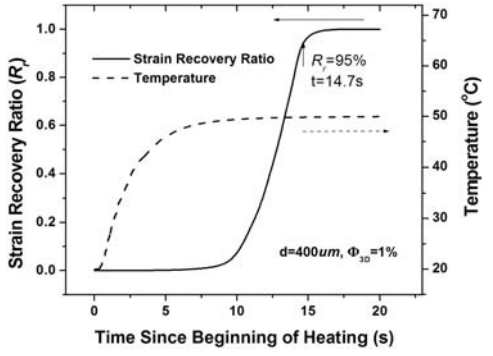

Figure 4. The strain recovery ratio and temperature of the 3D representative volume element (RVE) during the free recovery process. Note: temperature data is collected on point A on the 3D RVE.

the RVE boundaries. Second, the volume expansion of the material inside the RVE is hindered, leading to a high hydraulic pressure developed around the particle-matrix interface. This phenomenon could be visualized in Figure 6 where the evolution of hydraulic pressure (calculated as the negative summation of principle stresses, i.e. $p = -(\sigma_{11} + \sigma_{22} + \sigma_{33})$) at the particle interface is plotted as a function of time. It is noted that a negative pressure is also developed following the peak of the hydraulic pressure. Although the existence of hydraulic pressure may help retard interfacial defects, the negative pressure may initiate cracks.

Influence of particle size on the shape recovery rate

By further decreasing the diameter of magnetic particles to 200 μm and 1 μm, respectively, the influence of

particle size on the shape recovery rate of the SMP composite was investigated. Other parameters were the same as those in the representative case. The strain recovery ratio since beginning of heating, as well as the temperature at point A on the 3D RVE, is plotted in Figure 7. Table 2 lists the times for point A (furthest point to the center of RVE) to reach the target temperature (50°C) for the cases with different particle sizes and volume fractions. Two interesting trends can be observed. First, under a fixed volume fraction, increasing the particle size increases heating time. According to equation (23), as the particle diameter increases, the corresponding RVE edge length increases, so does the thermal conductive pathway. Therefore, more time is consumed for heat transfer before the external SMP material softens so that the elastic energy stored in the internal SMP material can be released and the shape can be recovered. In this case, the heat transfer is considered to be the governing factor in determining the recovery time. Second, when the particle size becomes small, heating becomes almost instantaneous. For example, at 0.1% volume fraction, 10 μm particles can heat the material in less than 0.01 s whilst 1 μm particles can do so in less than 0.002 s. For regular applications, however, the difference may not be distinguishable as they both are very fast.

Influence of particle volume fraction on the shape recovery rate

To study the influence of particle volume fraction on the shape recovery rate, the magnetic particle size was fixed as 1 μm during the finite element calculation whilst the particle volume fraction was varied as 0.1%, 1% and 10%, respectively. According to equation (23), when the volume fraction is increased at a specified particle diameter, the corresponding 3D RVE edge length is decreased. In this manner, the length of the thermal conductive pathway within the model is reduced, subsequently leading to a short recovery time of the SMP composite. As shown in Figure 8, when the particle volume fraction increases to 10% from 0.1%, the corresponding recovery time is reduced to 1.12 s from 1.38 s. Even though the demonstrated decrease in recovery time is minor in the presented

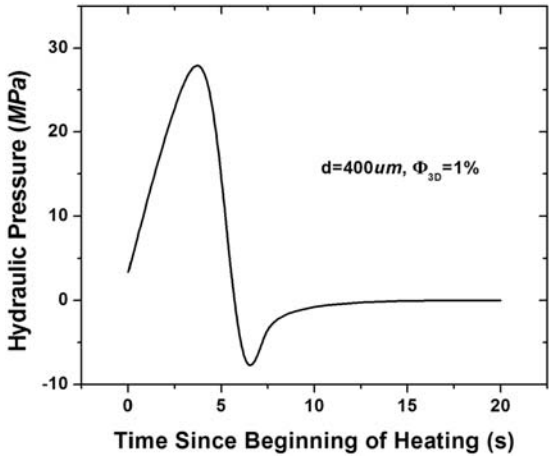

Figure 6. Hydraulic pressure evolution on the curved surface of 3D representative volume element (RVE) during the particle heating process.

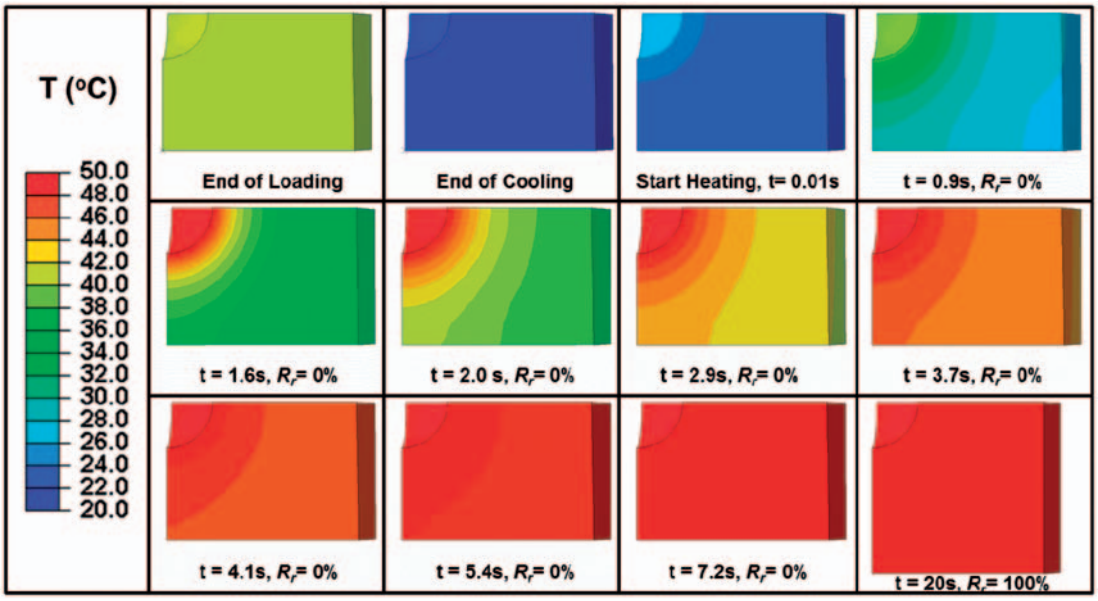

Figure 5. Temperature distribution within the 3D representative volume element (RVE) during the finite element analysis.

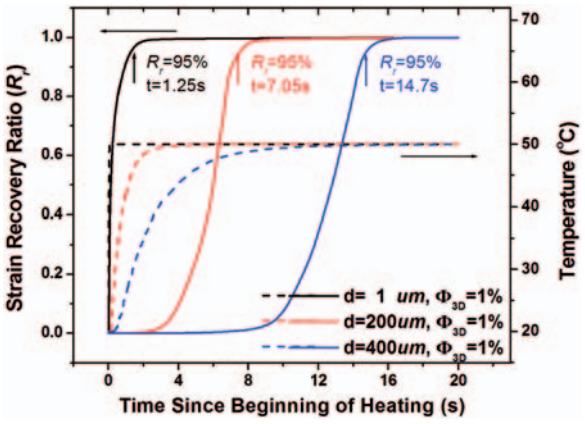

Figure 7. Strain recovery rate and temperature evolution of the shape memory polymer (SMP) composites reinforced by magnetic particles with uniform volume fraction but different sizes. Note: temperature data is collected on point A on the 3D representative volume element (RVE).

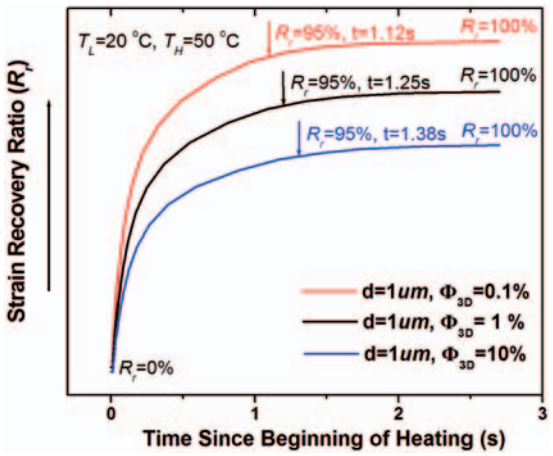

Figure 8. Strain recovery rate of the shape memory polymer (SMP) composites reinforced by magnetic particles with uniform size but different volume fractions. Note: The curves were slightly shifted vertically for better visualization.

Table 2. Heating times as a function of particle size and volume fraction

Particle diameter (μm)	$\phi_{3D} = 0.1\%$	$\phi_{3D} = 1\%$	$\phi_{3D} = 10\%$
1	0.00166 s	0.0015 s	0.00134 s
10	0.0097 s	0.0087 s	0.0069 s
40	0.106 s	0.06 s	0.031 s
100	3.71 s	1.07 s	0.32 s
200	11.3 s	2.85 s	0.66 s
400	60.3 s	7.42 s	1.27 s
1000	593 s	49.7 s	4.06 s

Note. The heating time is taken as when point A on the 3D representative volume element (RVE) reaches the target temperature (50°C).

comparison, it is expected to be more considerable in SMP composites containing larger-sized magnetic particles. This is because as the particle size increases, the effective thermal pathway will increase and thermal conduction becomes the dominating factor. This trend can also be seen in Table 2. Similar phenomenon was also observed by Yakacki et al.[32]

Critical particle sizes

As shown above, as the particle size becomes smaller, time for heat transfer becomes very small and thus heating becomes instantaneous. In this case, the dominating factor in determining recovery time is material recovery time under isothermal condition. Here, we call the recovery time under isothermal condition the intrinsic recovery time as it is determined solely by material properties. Therefore, there should exist a critical particle size, below which, shape recovery time is determined by the intrinsic recovery time. To further explore this critical particle size, Figure 9 shows the effects of particle sizes on the shape recovery time of the SMP composites. For each curve in Figure 9, a critical diameter can be observed, below which the time for full recovery is independent of the particle diameter. The critical diameters for the 0.001%, 0.1%, 1% and 10% volume fractions are approximately 0.15 μm, 1.7 μm, 7 μm and 80 μm for recoveries at 50°C, and 0.8 μm, 13 μm, 40 μm and 200 μm for recoveries at 40°C, respectively. The existence of the critical particle diameters could be well explained by the previous discussions and is considered to represent a threshold of recovery from one dominated by heat transfer to one dominated by material intrinsic recovery. At a specified particle volume fraction, the 3D RVE dimension decreases along with the decrease of particle size, and thus the shape recovery time is effectively reduced as a result of the reduction of the length of the thermal pathway. Below the critical particle size, the dimension of the 3D RVE becomes unimportant as heating can occur almost instantaneously. Therefore, from heating efficiency and material recovery points of view, it is unnecessary to further reduce the particle diameter. However, from the fabrication point of view, small particles could be easily suspended in solution than large particles and hence might be preferred. In such a case, the particle volume fraction can be reduced. For example, if the target recovery temperature is 50°C and particle size of 0.15 μm in diameter is used, only a 0.001% of volume fraction is necessary. Further increasing the volume fraction will not improve the heating efficiency.

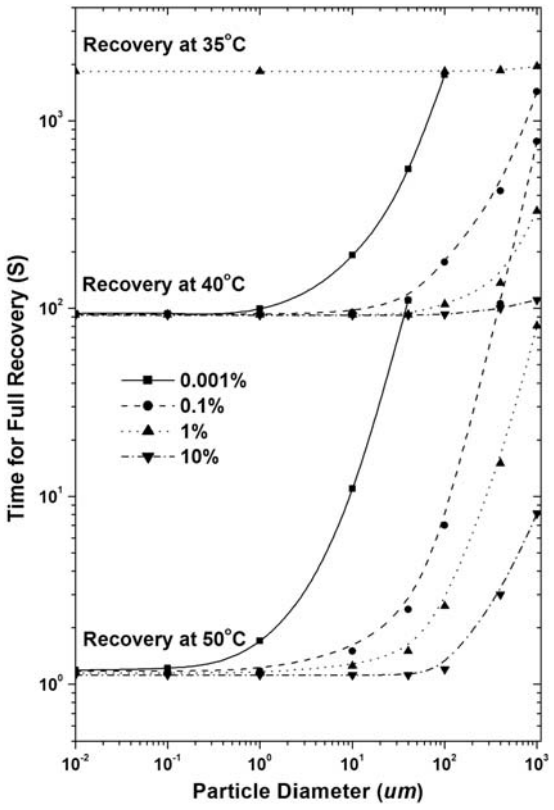

Figure 9. Prediction of critical particle diameters by showing effect of particle size on shape recovery time of the shape memory polymer (SMP) composites.

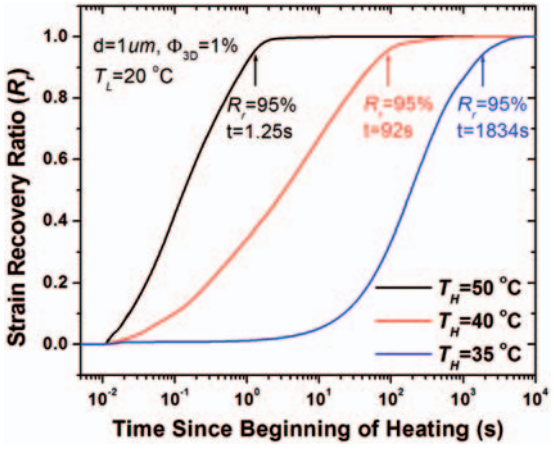

Figure 10. Strain recovery rate of the shape memory polymer (SMP) composites reinforced by magnetic particles with different particle heating temperature.

Influence of particle heating temperature and rate on the shape recovery rate

The influence of particle heating temperature on the shape recovery rate of the SMP composite was investigated. In the finite element simulation, while the particle diameter and volume fraction were fixed as 1 μm and 0.1%, respectively, the targeted high temperature achieved by magnetic particle were chosen as 35°C, 40°C and 50°C, respectively. Figure 10 shows the strain recovery as a function of time. At the temperature of 35°C, it takes 1834 s for 95% of shape recovery. Note that with 1 μm and 0.1% particle volume fraction, the SMP matrix reaches a uniform temperature within 0.0015 s (see Table 2). Therefore, in these cases, heat transfer is no longer the dominating factor on the shape recovery rate of SMP, but the material intrinsic recovery behavior dominates. Generally, the shape recovery rate of SMP composite would be increased under a higher heating temperature (i.e. a stronger external magnetic field). This tendency is consistent with the testing results reported by Kumar et al.[49] and Weigel et al.[50]

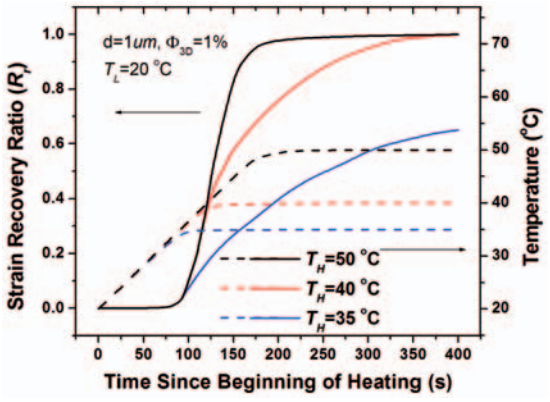

Figure 11. Strain recovery rate of the shape memory polymer (SMP) composites under a particle heating rate of 10°C/min and different target temperature.

In the above finite element simulations, the temperature of the magnetic particles was ramped to the target temperature (T_H) within 0.1 ms under the action of external electromagnetic filed. However, in practical applications, the particle temperature may not rise instantaneously from the energy consumption point of view. Therefore, we considered a case where the temperature of the magnetic particle was ramped at a rate of 10°C/min to the temperatures of 35°C, 40°C and 50°C, respectively. The particle diameter and volume fraction were still set as 1 μm and 1%. The time-dependent shape recovery behavior of the SMP composite is described in Figure 11, where the temperature is measured at point A. It is seen that the shape recovery does not start until the temperature reaches ~33°C. It is also interesting to note that under the same heating rate, the recoveries of the SMP with target temperature of 35°C and 40°C follow the same path of 50°C recovery until the respective target temperatures are reached, then the

recoveries becomes slow. Similar phenomenon was observed for an epoxy-based SMP.[47]

Conclusions

In this paper, finite element simulations were used to study the shape recovery behaviors of magnetic particle reinforced SMP composites. The finite element model was facilitated by a recently developed multi-branch thermoviscoelastic constitutive model for SMP. The required model parameters were experimentally determined by using experimental data from an acrylate-based SMP. Parametric studies were conducted to investigate some considerations should be followed in the designs of the SMP composites with magnetic particles. In general, reducing particle sizes or increase volume fractions can promote faster recovery rate. However, it was found that for a given target recovery temperature and a given particle volume fraction, there exists a critical particle size. For particle smaller than this critical size, the recovery time is dominated by the material intrinsic recovery time and is therefore independent of particle size. Similarly, for a given particle size and target recovery temperature, there exists a critical volume fraction. Above this volume fraction, further increasing volume fraction does not improve the heating efficiency.

Funding

We gratefully acknowledge the support of a NSF career award (CMMI-0645219), an AFOSR grant (FA9550-09-1-0195; Dr. Les Lee, program manager) and a NSF-Sandia initiative (Sandia National Laboratories, 618780).

Conflict of interest

None declared.

References

1. Xie T. Recent advances in polymer shape memory. *Polymer* 2011; 52: 4985–5000.
2. Lendlein A and Kelch S. Shape-memory polymers. *Angew Chem Int Ed Engl* 2002; 41(12): 2035–2057.
3. Liu C, Qin H and Mather PT. Review of progress in shape-memory polymers. *J Mater Chem* 2007; 17(16): 1543–1558.
4. Chung T, Rorno-Uribe A and Mather PT. Two-way reversible shape memory in a semicrystalline network. *Macromolecules* 2008; 41(1): 184–192.
5. Gall K, Yakacki CM, Liu YP, et al. Thermomechanics of the shape memory effect in polymers for biomedical applications. *J Biomed Mater Res Part A* 2005; 73A(3): 339–348.
6. Mather PT, Luo X and Rousseau IA. Shape memory polymer research. *Ann Rev Mater Res* 2009; 39: 445–471.
7. He Z, Satarkar N, Xie T, et al. Remote controlled multi-shape polymer nanocomposites with selective radiofrequency actuations. *Adv Mater* 2011; 23: 3192–3196.
8. Kumar UN, Kratz K, Wagermaier W, et al. Non-contact actuation of triple-shape effect in multiphase polymer network nanocomposites in alternating magnetic field. *J Mater Chem* 2010; 20: 3404–3415.
9. Jiang HY, Kelch S and Lendlein A. Polymers move in response to light. *Adv Mater* 2006; 18(11): 1471–1475.
10. Koerner H, Price G, Pearce NA, et al. Remotely actuated polymer nanocomposites – stress-recovery of carbon-nanotube-filled thermoplastic elastomers. *Nat Mater* 2004; 3(2): 115–120.
11. Lendlein A, Jiang H, Jünger O, et al. Light-induced shape-memory polymers. *Nature* 2005; 434(7035): 879–882.
12. Li MH, Keller P, Li B, et al. Light-driven side-on nematic elastomer actuators. *Adv Mater* 2003; 15(7–8): 569–572.
13. Scott TF, Draughon RB and Bowman CN. Actuation in crosslinked polymers via photoinduced stress relaxation. *Adv Mater* 2006; 18(16): 2128–2132.
14. Scott TF, Schneider AD, Cook WD, et al. Photoinduced plasticity in cross-linked polymers. *Science* 2005; 308(5728): 1615–1617.
15. Huang WM, Yang B, An L, et al. Water-driven programmable polyurethane shape memory polymer: Demonstration and mechanism. *Appl Phys Lett* 2005; 86(11): 114105.
16. Jung YC, So HH and Cho JW. Water-responsive shape memory polyurethane block copolymer modified with polyhedral oligomeric silsesquioxane. *J Macromol Sci Part B-Phys* 2006; 45(4): 453–461.
17. Wei ZG, Sandstrom R and Miyazaki S. Shape-memory materials and hybrid composites for smart systems I. Shape-memory materials. *J Mater Sci* 1998; 33(15): 3743–3762.
18. Yakacki CM, Shandas R, Lanning C, et al. Unconstrained recovery characterization of shape-memory polymer networks for cardiovascular applications. *Biomaterials* 2007; 28(14): 2255–2263.
19. Lendlein A and Kelch S. Shape-memory polymers as stimuli-sensitive implant materials. *Clin Hemorheol Microcirc* 2005; 32(2): 105–116.
20. Liu YP, Gall K, Dunn ML, et al. Thermomechanics of shape memory polymers: Uniaxial experiments and constitutive modeling. *Int J Plasticity* 2006; 22(2): 279–313.
21. Liu YP, Gall K, Dunn ML, et al. Thermomechanics of shape memory polymer nanocomposites. *Mech Mater* 2004; 36(10): 929–940.
22. Tobushi H, Hara H, Yamada E, et al. Thermomechanical properties in a thin film of shape memory polymer of polyurethane series. *Smart Mater Struct* 1996; 5(4): 483–491.
23. Cho JW, Kim JW, Jung YC, et al. Electroactive shape-memory polyurethane composites incorporating carbon nanotubes. *Macromol Rapid Commun* 2005; 26: 412–416.
24. Sahoo NG, Jung YC and Cho JW. Electroactive shape memory effect of polyurethane composites filled with carbon nanotubes and conducting polymer. *Mater Manuf Process* 2007; 22: 419–423.

25. Yu K, Zhang ZC, Liu YJ, et al. Carbon nanotube chains in a shape memory polymer/carbon black composite: to significantly reduce the electrical resistivity. *Appl Phys Lett* 2011; 98: 074102.
26. Schmidt AM. Electromagnetic activation of shape memory polymer networks containing magnetic nanoparticles. *Macromol Rapid Commun* 2006; 27(14): 1168–1172.
27. Buckley PR, McKinley GH, Wilson TS, et al. Inductively heated shape memory polymer for the magnetic actuation of medical devices. *IEEE Transact Biomed Eng* 2006; 53(10): 2075–2083.
28. Mohr R, Kratz K, Weigel T, et al. Initiation of shape-memory effect by inductive heating of magnetic nanoparticles in thermoplastic polymers. *PNAS* 2006; 103: 3540–3545.
29. Razzaq MY, Anhalt M, Frormann L, et al. Thermal, electrical and magnetic studies of magnetite filled polyurethane shape memory polymers. *Mater Sci Eng A* 2007; 444: 227–235.
30. Nikitina LV, Stepanovb GV, Mironovaa LS, et al. Magnetodeformational effect and effect of shape memory in magnetoelastics. *J Magn Magn Mater* 2004; 272: 2072–2073.
31. Weigel T, Mohr R and Lendlein A. Investigation of parameters to achieve temperatures required to initiate the shape-memory effect of magnetic nanocomposites by inductive heating. *Smart Mater Struct* 2009; 18(2): 025011.
32. Yakacki CM, Satarkar NS, Gall K, et al. Shape-memory polymer networks with fe_3O_4 nanoparticles for remote activation. *J Appl Polym Sci* 2009; 112(5): 3166–3176.
33. Westbrook KK, Kao PH, Castro F, et al. A 3D finite deformation constitutive model for amorphous shape memory polymers: a multi-branch modeling approach for nonequilibrium relaxation processes. *Mech Mater* 2011; 43: 853–869.
34. Holzapfel GA. *Nonlinear solid mechanics: a continuum approach for engineering*. Chichester, NY: Wiley, 2000.
35. Tool AQ. Relation between inelastic deformability and thermal expansion of glass in its annealing range. *J Am Ceram Soc* 1946; 29(9): 240–253.
36. Tool AQ. Effect of heat-treatment on the density and constitution of high-silica glasses of the borosilicate type. *J Am Ceram Soc* 1948; 31(7): 177–186.
37. Tool AQ and Eichlin CG. Variations caused in the heating curves of glass by heat treatment. *J Am Ceram Soc* 1931; 14(4): 276–308.
38. Kovacs AJ, Aklonis JJ, Hutchinson JM, et al. Isobaric volume and enthalpy recovery of glasses. II. A transparent multiparameter theory. *J Polym Sci, Polym Phys Ed* 1979; 17(7): 1097–1062.
39. Arruda EM and Boyce MC. A 3-dimensional constitutive model for the large stretch behavior of rubber elastic-materials. *J Mech Phys Solids* 1993; 41(2): 389–412.
40. Rubinstein M and Colby RH. *Polymer physics*. Oxford, NY: Oxford University Press, 2003.
41. Boyce MC, Parks DM and Argon AS. *Computational modeling of large strain plastic-deformation in glassy-polymers*. Abstracts of Papers of the American Chemical Society 196, 156-POLY, 1988.
42. Williams ML, Landel RF and Ferry JD. Temperature dependence of relaxation mechanisms in amorphous polymers and other glass-forming liquids. *Phys Rev* 1955; 98(5): 1549–1549.
43. Di Marzio EA and Yang AJM. Configurational entropy approach to the kinetics of glasses. *J Res Natl Instit Stand Technol* 1997; 102(2): 135–157.
44. Treloar LRG. *The physics of rubber elasticity*. Oxford: Clarendon Press, 1958.
45. Westbrook KK, Castro F, Long KN, et al. Improved testing system for thermomechanical experiments on polymers using uniaxial compression equipment. *Polym Test* 2010; 29(4): 503–512.
46. Qi HJ, Nguyen TD, Castro F, et al. Finite deformation thermo-mechanical behavior of thermally induced shape memory polymers. *J Mech Phys Solids* 2008; 56: 1730–1751.
47. Castro F, Westbook KK, Hermiller J, et al. Time and temperature dependent recovery of epoxy-based shape memory polymer. *ASME J Eng Mater Technol* 2011; 133(2): 021025.
48. Lendlein A and Langer R. Biodegradable, elastic shape-memory polymers for potential biomedical applications. *Science* 2002; 296(5573): 1673–1676.
49. Kumar UN, Kratz K, Heuchel M, et al. Shape-memory nanocomposites with magnetically adjustable apparent switching temperatures. *Adv Mater* 2011; 23: 4157–4162.
50. Weigel T, Mohr R and Lendlein A. Investigation of parameters to achieve temperatures required to initiate the shape-memory effect of magnetic nanocomposites by inductive heating. *Smart Mater Struct* 2009; 18: 025011.

Appendix A: Method for calculating the degree of the volume departure from equilibrium

The KAHR 33-parameter theory defines the evolution of δ by,

$$\delta = \sum_{j=1}^{33} \delta_j, \tag{A1a}$$

$$\frac{d\delta_j}{dt} = -3g_j\Delta\alpha\frac{dT}{dt} - \frac{\delta_j}{\tau_V^j(T,\delta)}, \tag{A1b}$$

$$g_j = \frac{0.15}{16} \quad \text{for } j \le 16 \text{ and } g_j = 0.05 \quad \text{for } j \ge 17, \tag{A1c}$$

where $\Delta\alpha = \alpha_r - \alpha_g$, α_g is the linear glassy CTE and τ_V^j is the structural relaxation time of the jth region and it is a function of current T and δ. According to the KAHR model, the structural relaxation time of the jth region is given by

$$\tau_V^j(T,\delta) = \tau_{V_0}^j b_T b_\delta, \tag{A2a}$$

$$b_T = \exp[-\theta(T - T_V)], \tag{A2b}$$

$$b_\delta = \exp[-(1 - x)\theta\delta/\Delta\alpha], \tag{A2c}$$

where $\tau^j_{V_0}$ is the relaxation time in equilibrium at the reference temperature T_V, b_T is a shift factor that incorporates the temperature dependence of τ^j_V at equilibrium (considered constant δ) through the parameter θ and b_δ is a second shift factor that incorporates the effect of the structure-dependent adjustment on the time scale. To control the degree of the contribution from temperature and structure to τ^j_V, the parameter x in equation (A2c) is used that ranges in value from 0 and 1. The structural relaxation times are equally distributed in logarithmic space over four decades with a median value of $\tau^{j=17}_{V_0} = \tau_V$. As a consequence, the fastest structural relaxation time $\tau^{j=1}_{V_0} = 0.01\tau_V$ and the slowest $\tau^{j=33}_{V_0} = 100\,\tau_V$.